Improve Control to Output Dynamic Response and Extend Modulation Index Range With Hybrid Selective Harmonic Current Mitigation-PWM and Phase-Shift PWM for Four-Quadrant Cascaded H-Bridge Converters

Amirhossein Moeini, *Student Member, IEEE*, Hui Zhao, *Student Member, IEEE*, and Shuo Wang, *Senior Member, IEEE*

***Abstract*—The selective harmonic current mitigation pulsewidth modulation (SHCM-PWM) technique can be used in cascaded multilevel converters to extend the harmonic reduction spectrum, reduce the coupling inductance and increase the efficiency. The offline SHCM-PWM technique has small number of switching transitions as its switching angles can only change once in a fundamental cycle and relatively long time delays because it uses FFT. As a result, its dynamic response has a lot to desire. As it will be proven in this paper, in four-quadrant power converters, to have a good transient dynamic response, both active and reactive power must be controlled at least two times in a fundamental cycle. In this paper, a hybrid modulation technique is introduced. The proposed technique uses SHCM-PWM under steady state and phase-shift PWM (PSPWM) under transient. In addition, in order to extend the modulation index range and ensure that SHCM-PWM can process four-quadrant active and reactive power, the constraints of the switching angles for the SHCM-PWM are modified. Simulations and experiments are conducted on a seven-level cascaded H-bridge converter to verify the proposed technique.**

***Index Terms*—Dynamic response, extended modulation index range, four-quadrant power converters, hybrid modulation technique, phase-shift pulsewidth modulation (PSPWM), selective harmonic current mitigation-PWM (SHCM-PWM).**

I. Introduction

MULTILEVEL power converters have drawn a lot of attentions nowadays [1], [2]. The modulation technique used in multilevel converters must have high efficiency, reduced passive filter cost, and fast transient response under different dynamic conditions [2], [3].

Manuscript received November 10, 2016; revised February 3, 2017; accepted February 20, 2017. Date of publication March 22, 2017; date of current version August 9, 2017. This work was supported by the National Science Foundation under Award 1540118. *(Corresponding author: Shuo Wang.)*

The authors are with the Department of Electrical and Computer Engineering, University of Florida, Gainesville, FL 32603 USA (e-mail: ahm1367@ufl.edu; zhaohui@ufl.edu; shuowang@ieee.org).

Color versions of one or more of the figures in this paper are available online at http://ieeexplore.ieee.org.

Digital Object Identifier 10.1109/TIE.2017.2686339

High efficiency is a critical metric [3] for multilevel converters. Because low switching frequencies lead to low switching power losses, the low switching frequency modulation techniques such as selective harmonic elimination-PWM (SHE-PWM) [4], selective harmonic mitigation-PWM (SHM-PWM) [5], and selective harmonic current mitigation-PWM (SHCM-PWM) [6] are promising to increase converter efficiencies.

In conventional SHE-PWM or SHM-PWM techniques, only the low-order harmonics are eliminated or mitigated to meet voltage harmonic limits [3]. Hence, the conventional SHE-PWM and SHM-PWM techniques cannot ensure to meet the current harmonic limits, which are more important than the voltage harmonic limits for the grid tied converters [6]. In addition, the grid voltage harmonics can lead to unmitigated current harmonics for SHE-PWM and SHM-PWM techniques, but this information is not included in the equations of these modulation techniques.

These two problems have been solved in [6] by introducing SHCM-PWM technique that can meet the current harmonic limits of IEEE-519 [7] by including the effects of the grid voltage harmonics in the optimization process. In this technique, the coupling inductance between the converter and the grid can be significantly reduced in comparison to SHE-PWM and SHM-PWM techniques [6]. Moreover, higher number of current harmonics than SHE-PWM and SHM-PWM techniques can be mitigated with the same number of switching transitions [6].

In [8] and [9], it has been proven that the dynamic performance of low-frequency SHE-PWM technique is weak due to using FFT block in single-phase grid-tied converters. As a result, at least one fundamental cycle is required to change modulation index with SHE-PWM technique. Furthermore, this technique does not control four-quadrant active and reactive power in grid-tied converters. It does not guarantee to meet the current limits of IEEE-519 too.

In [3], based on the dynamic equations of grid-tied converters, a high-performance dynamic response has been achieved for the four-quadrant grid-tied converter. In addition, an indirect controller is used to change the active and reactive currents four times in each fundamental cycle. The modulation technique used in [3] is phase-shift PWM (PSPWM). It uses a high switching frequency to control low-order harmonics. It is important to note that the SHCM-PWM technique could not be used with the indirect controller technique to obtain high dynamic performance. The SHCM-PWM is an off-line modulation technique because the switching angles are calculated and stored in lookup tables. It also uses FFT, which results in time delays. In addition, the number of switching transitions is very low in SHCM-PWM, so it intrinsically has weak dynamic performance [8]. When active or reactive power are controlled with SHCM-PWM in four-quadrant converters, because the switching angles need one fundamental cycle to get updated [8], a dc offset remains on the injected currents for several cycles under dynamic conditions [3].

Grid-tied four-quadrant converters need large modulation index range to work with different active and reactive loads [9]. The modulation index range of low-frequency modulation techniques depends on optimization constraints applied to the Fourier series equations. To increase modulation index range of low-frequency modulation techniques, either unequal dc-link voltage technique [11] or modified switching angle constraints [10] can be used.

In this paper, a hybrid modulation technique, which combines SHCM-PWM and PSPWM, is proposed to achieve high dynamic performance for four-quadrant grid-tied converters. Under steady state condition, SHCM-PWM technique is applied to achieve high efficiency. Under dynamic condition, the PSPWM technique is employed to update switching transitions several times in each fundamental cycle to achieve high dynamic response performance. Furthermore, a controller is designed to switch between these two modulations. In order to process four-quadrant active and reactive power, the modulation index range of SHCM-PWM is greatly extended by modifying the constraints of switching angles. The lowest number of switching transitions for PSPWM technique is derived so that it does not reduce efficiency and the performance of the proposed indirect controller.

II. Extend Modulation Index Range of SHCM-PWM for Four-Quadrant Converters

An example of the configuration of a four-quadrant cascaded H-bridge (CHB) grid-tied converter is shown in Fig. 1. The CHB converter is connected to a power grid with coupling inductance L_F and parasitic resistance R_F. The CHB converter consists of i number of cells. The dc-link voltages are equal to $V_{\rm dc}$. The DC side of each cell is directly connected to the isolated dc/dc converters. The outputs of isolated dc/dc converters are paralleled to charge energy storage on a dc bus. The loads can be connected to dc bus with bi-directional dc/dc converters in Fig. 1. Because dc-link voltages of CHB converter can be regulated with the isolated dc/dc converters [12], in this paper, the dc links are connected to dc sources, which will not invalidate the proposed technique. The time-domain current equation of the

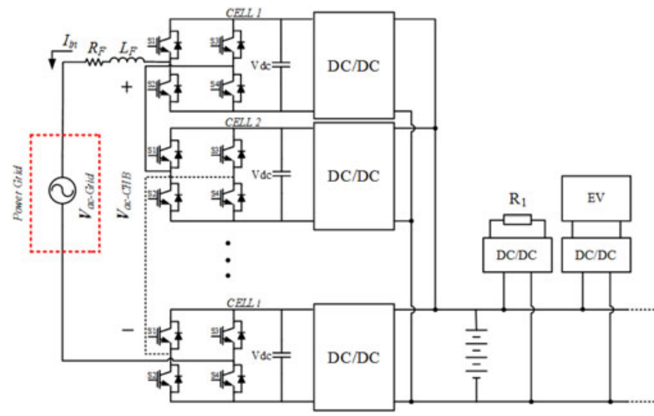

Fig. 1. Configuration of a four-quadrant grid-tied CHB converter.

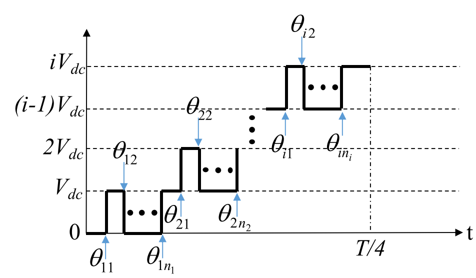

Fig. 2. Voltage waveform of an *i*-cell SHCM-PWM converter.

CHB converter on ac side is

$$v_{\text{ac-CHB-}h}(t) = L_F \frac{di_{\text{in-}h}(t)}{dt} + R_F i_{\text{in-}h}(t) + v_{\text{ac-Grid-}h}(t). \quad (1)$$

In (1), $v_{\text{ac-Grid-}h}$, $v_{\text{ac}-\text{CHB-h}}$, and $i_{\text{in-}h}$ are the hth harmonic order of the grid voltage, CHB voltage, and injected current, respectively. The relationship of the fundamental frequency (60/50 Hz) component $v_{\text{ac-Grid-1}}$, $v_{\text{ac-CHB-1}}$, and $i_{\text{in-1}}$ can be obtained in (1). The quarter period waveform of $v_{\text{ac-CHB-}h}$ for the *i*-cell CHB converter in Fig. 1, when jth cell has n_j $(j = 1, 2, \ldots, i)$ switching angles in each quarter period, is shown in Fig. 2. Due to quarter wave symmetry, the Fourier series equations of Fig. 2 can be written as

$$v_{\text{ac-CHB}}(t) = \sum_{h=1}^{\infty} \frac{4V_{\rm dc}}{\pi h} b_h \sin(h\omega t)$$

$$b_h = (\cos(h\theta_{11}) - \cos(h\theta_{12}) + \cdots + \cos(h\theta_{i(n_i)})) \quad (2)$$

where $\theta_{11}, \theta_{12}, \ldots, \theta_{i(n_i)}$ are the switching angles of the CHB converter in each quarter period as shown in Fig. 2. $4V_{\rm dc} b_h/(\pi h)$ is the magnitude of the hth-order harmonic for $v_{\text{ac-CHB}}(t)$. When $h = 1$, the modulation index $(M_a = b_1)$ of CHB converter is obtained from (2).

The power quality standard that is used in this paper to meet both current and voltage harmonics is IEEE 519 [7]. The limits of both current and voltage harmonics at the point of common coupling (PCC) are provided in Table I. In IEEE-519,

TABLE I
CURRENT AND VOLTAGE HARMONIC LIMITS OF THE IEEE 519 STANDARD [7] $(Isc/IL \leq 20)$ FOR GRID VOLTAGE LESS THAN 69 KV

Harmonic Order (h)	Current Harmonics and Total Demand Distortion (TDD)	Voltage Harmonics and Total Harmonic Distortion (THD)
$3 \leq h < 11$	4%	3%
$11 \leq h < 17$	2%	3%
$17 \leq h < 23$	1.5%	3%
$23 \leq h < 35$	0.6%	3%
$35 \leq h$	0.3%	3%
TDD or THD	5%	5%

TABLE II
CALCULATED CIRCUIT PARAMETERS OF SHCM-PWM TECHNIQUE

Parameter	Symbol	Value
Line frequency	F	60 Hz
AC grid Voltage (RMS)	$V_{\text{ac-Grid}}$	110 V
Total rated power	S_{total}	1.5 kVA
Maximum demand load (RMS)	I_L	14.14 A
Number of H-bridge cells	I	3
Number of switching transitions	K	9
Highest order of mitigated harmonic in (3)	H	69th
DC-bus voltage	V_{dc}	73 V
Coupling inductance	L_F	10 mH (0.485 p.u.)
Parasitic resistance of L_F	R_F	0.6 Ω

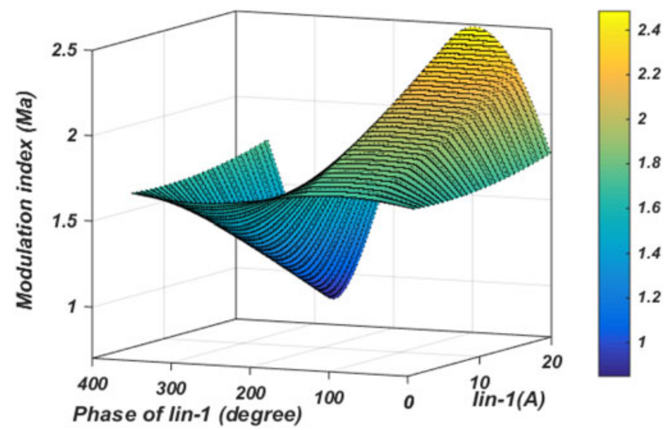

Fig. 3. Required modulation index for a four-quadrant CHB converter.

I_L is the maximum demand load current of the four-quadrant converter. I_{sc} is the short circuit current at the PCC.

Moeini *et al.* [6] discussed how to design the key parameters such as the switching frequency of each switch, the number of harmonics that can be mitigated with the SHCM-PWM, and the coupling inductance between the converter and the grid in details. When the grid voltage harmonics ($|V_{\text{ac-Grid-}h}|$) have the highest magnitudes under the worst scenario defined in Table I, the equation set that is used to find the solutions of SHCM-PWM to meet the current harmonic limits of IEEE 519 in Table I is given by

$$M_a = \cos\theta_{11} - \cos\theta_{12} + \cos\theta_{13} + \cdots + \cos\theta_K$$
$$\frac{|v_{\text{ac-Grid-}h}| + |v_{\text{ac-CHB-}h}|}{|\omega h L_T I_L|} \leq C_h, \qquad h = 3, 5, 7, \ldots$$
$$\sqrt{\left(\frac{I_{\text{in-3}}}{I_L}\right)^2 + \left(\frac{I_{\text{in-5}}}{I_L}\right)^2 + \cdots + \left(\frac{I_{\text{in-}h}}{I_L}\right)^2} \leq C_{\text{TDD}} \quad (3)$$

where K is the number of switching transitions of the SHCM-PWM during a quarter fundamental period ($K = n_{11} + n_{12} + \ldots + n_{i(ni)}$) and C_h and C_{TDD} are the current harmonics and TDD limits of i_{in} in Table I. By using guidelines in [6], the parameters are calculated in Table II.

To ensure that the proposed SHCM-PWM modulation technique can properly work in steady state for four-quadrant active and reactive power, the limitations for the maximum and minimum modulation indices can be obtained based on (1). In (1), the modulation index of CHB voltage is

$$M_a = |\frac{\pi}{4V_{\text{dc}}}(V_{\text{ac-Grid-1}}\angle 0 + (j\omega L_F + R_F)I_{\text{in-1}}\angle\theta_{I_{\text{in-1}}})|. \quad (4)$$

In (4), if the grid voltage is taken as the reference, by changing the magnitude and phase of $i_{\text{in-1}}$ ($0 < I_{\text{in-1}} < I_L$, $0 < \theta_{I_{\text{in-1}}} < 2\pi$), the required modulation indices are derived in Fig. 3, for the circuit parameters in Table II. As shown in this figure, the CHB converter can process four-quadrant active and reactive power at steady state when modulation indices changes from 0.85 to 2.485.

The conventional constraints of the switching angles used to solve switching angles for the equation set in (3) are

$$0 < \theta_{11} < \theta_{12} < \cdots < \theta_{\text{in}_i} < \frac{\pi}{2}. \quad (5)$$

The constraints in (5) undesirably restrict the optimization techniques used to solve the equation set (3). The switching angle solution range of SHCM-PWM technique can be significantly improved by modifying the constraints to

$$0 < \theta_{11} < \frac{\pi}{2}, 0 < \theta_{12} < \frac{\pi}{2}, \ldots, 0 < \theta_{\text{in}_i} < \frac{\pi}{2}. \quad (6)$$

For the modified switching angles in (6), due to the reduced constraints from (5), the switching sequences could be different from that in Fig. 2. For example, if θ_{12} is the first switching angle and θ_{11} is the second switching angle, at θ_{12}, the voltage will decrease from 0 to $-V_{\text{dc}}$ and at θ_{11}, the voltage will increase from $-V_{\text{dc}}$ to 0 [10].

As proven in [13] and [14], the particle swarm optimization (PSO) technique can find the solutions for low-frequency modulation techniques such as SHE-PWM, SHM-PWM, and SHCM-PWM faster with fewer computations than Genetic Algorithm or Newton−Raphson techniques. The multiobjective

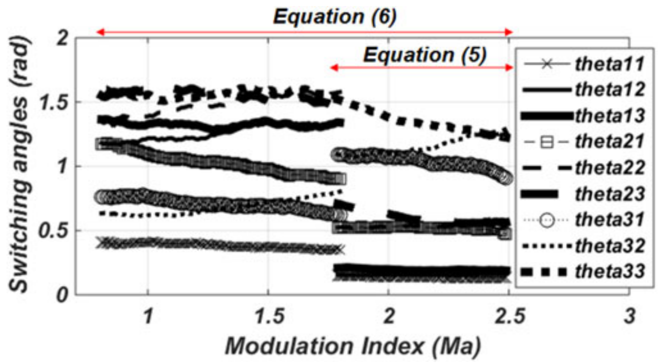

Fig. 4. Switching angle solutions versus modulation index with SHCM-PWM technique and constraint in (5) or (6).

PSO (MOPSO) technique [15] is used to solve the equation set (3) because of its advantages of mitigating each order harmonic current and TDD over PSO technique. The modulation index ranges of using the switching angle constraints in (5) and (6) for the equation set (3) are compared in Fig. 4. As shown in the figure, the switching angle solution with conventional constraints (5) limits the modulation index to [1.78, 2.495]. The modulation index is greatly extended to [0.8, 2.495] with the modified switching angle constraints (6). It covers all of the required modulation indices in Fig. 3. It is important to note that all the solutions in Fig. 4 are for three-cell CHB converters.

By changing the modulation index, the magnitude of $v_{\text{ac-CHB-1}}$ in (2) can be controlled. However, in order to track desired active and reactive power for four-quadrant operations, the phase of CHB voltage should also be controlled. Because of this, if the phase of the CHB voltage is θ and $0 < \theta < 2\pi$, (2) can be rewritten as

$$v_{\text{ac}-\text{CHB}}(t) = \sum_{h=1}^{\infty} \frac{4V_{\text{dc}}}{\pi h} b_h \sin(h\omega t + h\theta) \tag{7}$$

or

$$v_{\text{ac}-\text{CHB}}(t) = \sum_{h=1}^{\infty} \frac{4V_{\text{dc}}}{\pi h} b_h (\cos(h\theta)\sin(h\omega t) + \sin(h\theta)\cos(h\omega t)). \tag{8}$$

Because when the phases of both $i_{\text{in-1}}$ and $v_{\text{ac-CHB}}$ change from 0 to 2π, there are switching angle solutions for the CHB to handle four-quadrant active and reactive power.

III. Technique to Improve Transient Response in a Four-Quadrant Grid-Tied CHB Converter

A. Proposed Technique to Improve Transient Response with Hybrid SHCM-PWM and PSPWM Technique

In (1), the fundamental frequency of $i_{\text{in}}(t)$ for a single-phase CHB converter can be written as

$$i_{\text{in}}(t) = I_{\text{in-1}} \sin(\omega t + \theta_{I_{\text{in-1}}}). \tag{9}$$

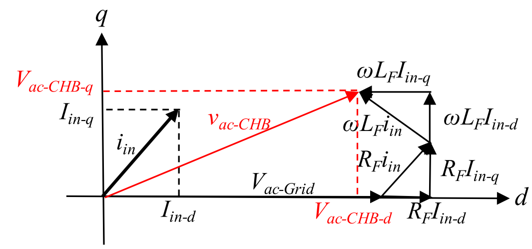

Fig. 5. Phasor diagram of the grid-tied converter.

By expanding (9), the following equation can be derived for the current of the single-phase CHB converter:

$$\begin{cases} i_{\text{in}}(t) = I_{\text{in-}d}\sin(\omega t) + I_{\text{in-}q}\cos(\omega t), \\ I_{\text{in-}d} = I_{\text{in-1}}\cos(\theta_{I_{\text{in-1}}}), \\ I_{\text{in-}q} = I_{\text{in-1}}\sin(\theta_{I_{\text{in-1}}}), \end{cases} \tag{10}$$

where d and q are used in (10) to simplify representation of $i_{\text{in}}(t)$. The dq phasor diagram of (1) and (10) for the fundamental frequency is shown in Fig. 5. In Fig. 5, the dq frame rotates in counterclockwise at speed ω. From Fig. 5, the CHB voltage is

$$\begin{aligned} v_{\text{ac-CHB}}(t) &= \omega L_F I_{\text{in-1}}\cos(\omega t + \theta_{I_{\text{in-1}}}) \\ &+ R_F I_{\text{in-1}}\sin(\omega t + \theta_{I_{\text{in-1}}}) + V_{\text{ac-Grid}}\sin(\omega t) \\ &= -L_F\omega I_{\text{in-}q}\sin(\omega t) + L_F\omega I_{\text{in-}d}\cos(\omega t) \\ &+ R_F I_{\text{in-}d}\sin(\omega t) + R_F I_{\text{in-}q}\cos(\omega t) + V_{\text{ac-Grid}}\sin(\omega t) \\ &= V_{\text{ac-CHB-}d}\sin(\omega t) + V_{\text{ac-CHB-}q}\cos(\omega t) \end{aligned} \tag{11}$$

where

$$\begin{aligned} V_{\text{ac-CHB-}d} &= -L_F\omega I_{\text{in-}q} + R_F I_{\text{in-}d} + V_{\text{ac-Grid}} \\ V_{\text{ac-CHB-}q} &= L_F\omega I_{\text{in-}d} + R_F I_{\text{in-}q}. \end{aligned}$$

In order to have the desired current in Fig. 5, the CHB voltage can be controlled with b_1 and θ in (8) by using the following equations:

$$\begin{aligned} V_{\text{ac-CHB-}d} &= \frac{4V_{\text{dc}}b_1}{\pi}\cos\theta \\ V_{\text{ac-CHB-}q} &= \frac{4V_{\text{dc}}b_1}{\pi}\sin\theta. \end{aligned} \tag{12}$$

In the time domain, if the changes of dq current references cause $v_{\text{ac\_CHB}}(t)$ to change by $\Delta v_{\text{ac\_CHB}}(t)$ from $v_{\text{ac\_CHB1}}(t)$ to $v_{\text{ac\_CHB2}}(t)$ and $i_{\text{in}}(t)$ to change by $\Delta i_{\text{in}}(t)$ from $i_{\text{in1}}(t)$ to $i_{\text{in2}}(t)$, the following equations hold:

$$\begin{aligned} i_{\text{in2}}(t) &= i_{\text{in1}}(t) + \Delta i_{\text{in}}(t) \\ v_{\text{ac-CHB2}}(t) &= v_{\text{ac-CHB1}}(t) + \Delta v_{\text{ac-CHB}}(t). \end{aligned} \tag{13}$$

It is assumed that the grid voltage does not change under the transient condition so $\Delta v_{\text{ac-Grid}} = 0$. Based on Fig. 5 and (10),

Δi_{in} and $\Delta v_{\text{ac-CHB}}$ can be derived as

$$\begin{aligned}\Delta V_{\text{ac-CHB-}d} &= -L_F\omega\Delta I_{\text{in-}q} + R_F\Delta I_{\text{in-}d}\\ \Delta V_{\text{ac-CHB-}q} &= L_F\omega\Delta I_{\text{in-}d} + R_F\Delta I_{\text{in-}q}\\ \Delta v_{\text{ac-CHB}}(t) &= \Delta V_{\text{ac-CHB-}d}\sin(\omega t)\\ &\quad + \Delta V_{\text{ac-CHB-}q}\cos(\omega t)\\ \Delta i_{\text{in}}(t) &= \Delta I_{\text{in-}d}\sin(\omega t) + \Delta I_{\text{in-}q}\cos(\omega t) \qquad (14)\end{aligned}$$

where Δi_{in} and $\Delta v_{\text{ac-CHB}}$ in (13) and (14) are the steady-state components of input current and CHB voltage. The differential equation under transient duration is

$$\Delta v_{\text{ac-CHB}}(t) = L_F\frac{d\Delta i_{\text{in}}(t)}{dt} + R_F\Delta i_{\text{in}}(t). \qquad (15)$$

If the current changes at $t = t_0$, from (14) and (15), Δi_{in} can be solved as

$$\Delta i_{\text{in}}(t) = ce^{\frac{-R_F}{L_F}t} + (\Delta I_{\text{in-}d}\sin(\omega t) + \Delta I_{\text{in-}q}\cos(\omega t)) \quad (16)$$

where c depends on both $\Delta v_{\text{ac-CHB}}$ and the initial condition of Δi_{in}. If the control signal of $\Delta I_{\text{in-}d}$ and $\Delta I_{\text{in}-q}$ change at $t = t_0$ and $\Delta i_{\text{in}}(t_0^-) = 0$, c can be derived as

$$c = -e^{\frac{R_F}{L_F}t_0}(\Delta I_{\text{in-}d}\sin(\omega t_0) + \Delta I_{\text{in-}q}\cos(\omega t_0)). \qquad (17)$$

The second term in (16) is the steady-state term of Δi_{in}. The first term in (16) is an undesirable transient current. In order to remove undesirable transient current, in (17), c should be always equal to zero. Because of this, $\Delta I_{\text{in-}d}$ or $\Delta I_{\text{in-}q}$ should only change when $\sin(\omega t_0)$ or $\cos(\omega t_0)$ are equal to zero. This indicates if dq currents in (17) change under the following conditions, i_{in} will have no transient currents:

$$\begin{cases}\omega t_0 = k\pi, & \Delta I_{\text{in-}d}\text{ should change}\\ \omega t_0 = k\pi + \frac{\pi}{2}, & \Delta I_{\text{in-}q}\text{ should change}\end{cases}. \qquad (18)$$

To have the fast transient response in practice, the active power, which is determined by $\Delta I_{\text{in-}d}$, and the reactive power, which is determined by $\Delta I_{\text{in-}q}$, must change at times defined in (18). Therefore, the currents can have two to four changes within one cycle. At the same time, the existing technique uses only PSPWM technique to improve the transient condition [3]. However, the mitigation of low-order current harmonics using PSPWM technique needs more switching transitions than low-frequency modulation techniques such as SHE-PWM or SHCM-PWM [6], [16]. As a result, PSPWM technique has high switching power loss. To solve this issue, a hybrid SHCM-PWM and PSPWM technique is proposed in this paper. In this technique, SHCM-PWM technique is employed under the steady-state condition and PSPWM technique is employed under the transient condition. The block diagram in Fig. 6 shows the proposed hybrid SHCM-PWM and PSPWM technique. In the figure, when current references $\Delta I^*_{\text{in-}d}$ and $\Delta I^*_{\text{in-}q}$ change, the following conditions must be used by the modulation selector to select the modulation technique for the CHB converter.

1) If $|\Delta I^*_{\text{in-}d}| > 0$ and $\omega t = k\pi$, use PSPWM (SW_{PS}) until $\omega t = (k+2)\pi$.

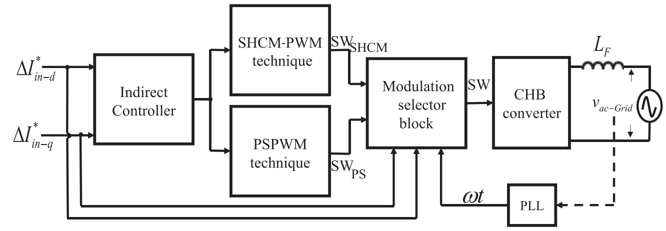

Fig. 6. Proposed hybrid SHCM-PWM and PSPWM controller.

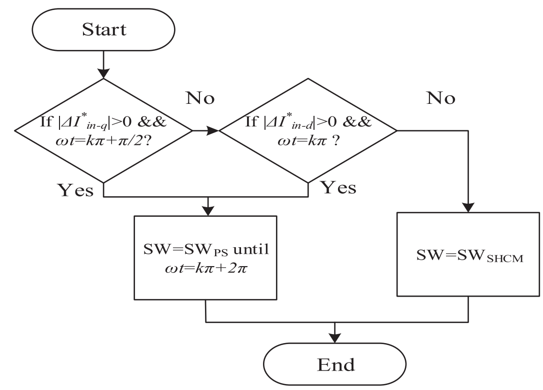

Fig. 7. Flowchart of modulation selector block in Fig. 6.

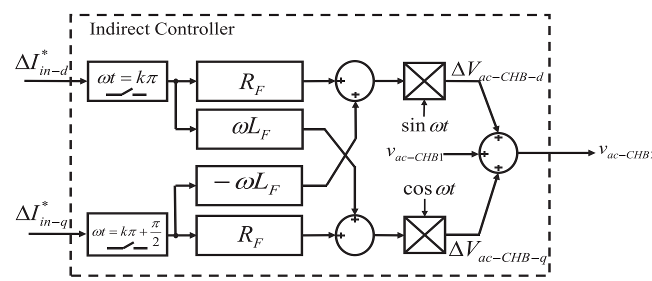

Fig. 8. Indirect controller which is used to generate $v_{\text{ac-CHB}}$ in [3].

2) If $|\Delta I^*_{\text{in-}q}| > 0$ and $\omega t = k\pi + \pi/2$, use PSPWM (SW_{PS}) until $\omega t = (k+2)\pi$.

3) Otherwise, use SHCM-PWM.

The flowchart for the modulation selector block in Fig. 6 is shown in Fig. 7 [3]. The block diagram of the indirect controller based on (13), (14), and (18) is shown in Fig. 8. The output of the indirect controller in Fig. 8 is $v_{\text{ac-CHB2}}$. Because PSPWM technique does not use fast Fourier transform (FFT) to change $v_{\text{ac-CHB}}$ [7], it is possible to change $v_{\text{ac-CHB}}$ several times in a fundamental period. On the other hand, the SHCM-PWM technique needs to use the FFT block to obtain the modulation index M_a, which is needed for checking look up tables and changing the output voltage of CHB converter [7]. Because the FFT block has time delays, SHCM-PWM technique needs at least one cycle to change $v_{\text{ac-CHB}}$. However, (18) requires to change the $v_{\text{ac-CHB}}$ at least twice in a fundamental period so both active and reactive power can be controlled for a four-quadrant grid-tied converter. Therefore, PSPWM technique is an appropriate technique for dynamic response improvement.

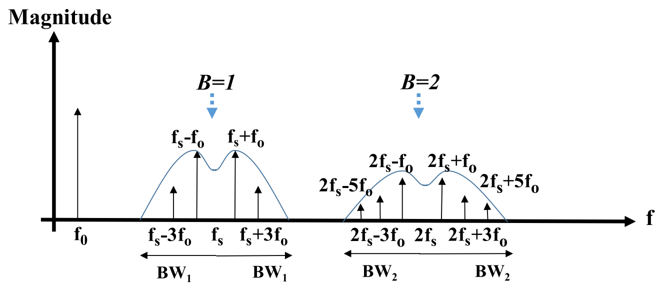

Fig. 9. Harmonic spectrum of $v_{\text{ac-CHB}}$ with PSPWM technique.

B. Design the Switching Frequency of PSPWM Technique

The switching frequency of PSPWM technique must be designed to have both good dynamic response and low switching power loss. To reduce the switching power loss, the switching frequency of PSPWM must be chosen as low as possible when the dynamic response is greatly improved. However, as shown in [8], reducing the switching frequency of PSPWM may lead to undesirable high low-order voltage harmonics, which includes the fundamental $v_{\text{ac-CHB-1}}$. Because of this, the lowest PSPWM switching frequency, which does not affect $v_{\text{ac-CHB-1}}$, is explored in this section. As discussed in [16], the output voltage of an *i*-cell CHB converter with the PSPWM technique can be written as

$$v_{\text{ac-CHB-PSPWM}}(t) = iV_{\text{dc}}M\cos(\omega_0 t + \theta_0) + \frac{4V_{\text{dc}}}{\pi}\sum_{B=1}^{\infty}\sum_{A=-\infty}^{\infty}\left(\frac{1}{2B}J_{2A-1}(iB\pi M)\right) \times \sin\left((2iB+2A-1)\frac{\pi}{2}\right)\cos(2iB\omega_c t + (2A-1)(\omega_0 t + \theta_0)) \tag{19}$$

where $\omega_0 = 2\pi f_0$, f_0 and θ_0 are the fundamental frequency and phase of CHB voltage. *M* is the modulation index of each cell of CHB. The total modulation index M_a of CHB converter is *iM*. $\omega_c = 2\pi f_c$ and f_c is the average carrier frequency of each cell. In Fig. 9, the BW_1 and BW_2 are the first and second base bands of PSPWM technique described in (20). The harmonics exist at $Bf_s \pm (2A+1)f_o$ orders. In (19), the total switching frequency f_s of all cells of $v_{\text{ac-CHB}}$ with PSPWM is equal to if_c. *B* is the baseband and *A* is the sideband harmonics of each baseband harmonic as shown in Fig. 9. *J* is the Bessel function of first kind. The bandwidth of Bth baseband harmonic in Fig. 9 can be obtained with the following equation [8]:

$$BW_B \approx 2(iMB\pi + 2)f_0. \tag{20}$$

In order not to generate sideband harmonics overlapping and influencing $v_{\text{ac-CHB-1}}$, the carrier frequency of CHB converter for first baseband $(B = 1)$ can be derived based on following equation:

$$f_s - BW_1 > f_0 \Rightarrow f_s > f_0 + BW_1 \Rightarrow f_s > (2iMB\pi + 5)f_0. \tag{21}$$

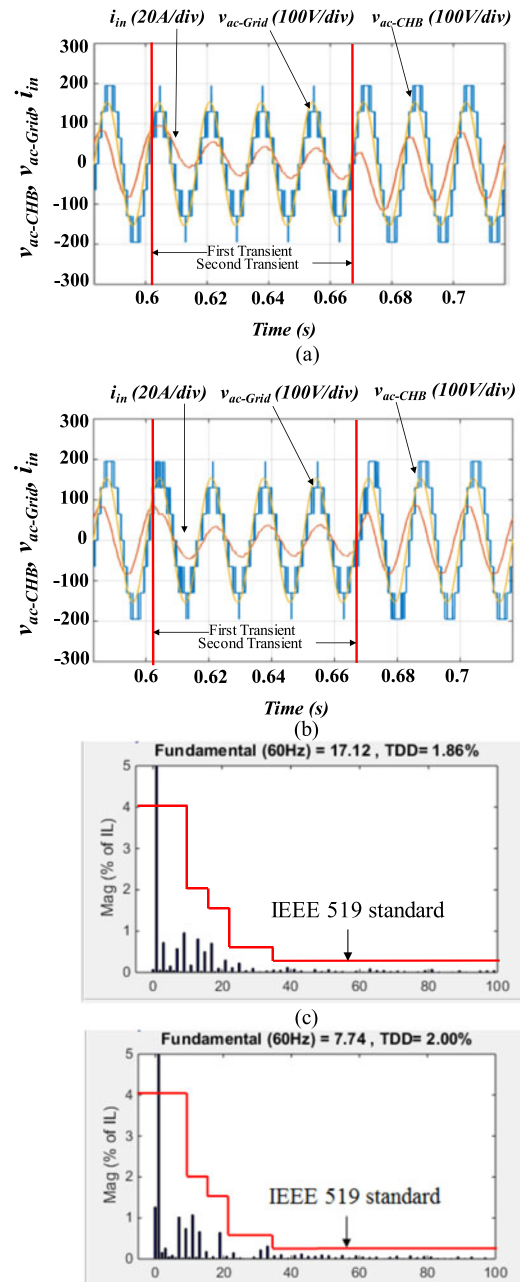

Fig. 10. Simulation results of the four-quadrant converter, when active and reactive power changes from 1000 W − 830 VAR to 520 W + 275 VAR and then back to 1000 W − 830 VAR: (a) $V_{\text{ac-CHB}}$, $V_{\text{ac-Grid}}$, I_{in} with conventional technique, (b) $V_{\text{ac-CHB}}$, $V_{\text{ac-Grid}}$, I_{in} with the proposed hybrid technique, (c) the harmonic spectrum at 1000 W − 830 VAR with the proposed hybrid technique, and (d) the harmonic spectrum at 520 W + 275 VAR with the proposed hybrid technique.

Based on (21), when $i = 3$, $M = 1$(the maximum modulation index for each cell) and in the worst scenario, the lowest f_s and f_c are therefore 720 and 240 Hz, respectively.

IV. Simulation Results

In order to validate the proposed hybrid SHCM-PWM and PSPWM technique, MATLAB Simulink is used for the simulations. The circuit parameters, which are used in both simulation

TABLE III
MAXIMUM DC OFFSET OF II_N IN SIMULATIONS WITH EITHER CONVENTIONAL OR PROPOSED TECHNIQUES

Comparative Simulations	First Transient (Conventional)	First Transient (Proposed)	Second Transient (Conventional)	Second Transient (Proposed)
1	78%	8.5%	43%	1.75%
2	92%	3.8%	94%	1.4%

TABLE IV
SWITCHING POWER LOSS OF CHB CONVERTER WITH SHCM-PWM TECHNIQUE

	1000 W − 830 VAR	520 W + 275 VAR	−800 W + 870 VAR	−500 W − 520 VAR
SHCM	0.131W	0.085W	0.103W	0.118W
PSPWM	1W	0.644W	0.787W	1.253W

and experimental results, are shown in Table II. The dc voltage of battery for each cell in the simulation and experimental results is 65 V. The obtained solutions in Fig. 4 can still be used for $V_{\rm dc} = 65$ V because low dc-link voltages result in low-voltage harmonics in (2) and (3). For a CHB cell with SHCM-PWM, a switching cycle is defined as a cycle in which each switch turns on and off once. This means the number of switching transitions of each cell in quarter fundamental period is equal to the number of switching cycles in one fundamental period of each cell. The total switching frequency of the CHB converter is therefore equal to the number of cells times the number of switching transitions in quarter fundamental period of each cell times the fundamental frequency. The total switching frequency of SHCM-PWM technique for a three-cell CHB converter is therefore 3 (transition) × 3 (cell) × 60 Hz = 540 Hz. For PSPWM technique, as discussed previously, the total switching frequency is 3 (cell) × 240 Hz = 720 Hz.

The purposes of the simulations and experiments are as follows.

1) Validating $i_{\rm in}$ can meet the IEEE 519 current harmonic limits with the extended solution range in (6).
2) Validating proposed hybrid SHCM-PWM and PSPWM techniques based on Fig. 6 can achieve high dynamic response and the transient current can be significantly reduced.
3) Validating CHB converter can process four-quadrant active and reactive power. The active and reactive powers can be either injected to or absorbed from the power grid.
4) Validating SHCM-PWM technique has a lower switching power loss than conventional PSPWM technique when both meet IEEE-519.

In the first comparative simulations, the active and reactive power flowing from power grid to the converter changed from 1000 W − 830 VAR to 520 W + 275 VAR at $t = 0.60231$ s and then changed back to 1000 W − 830 VAR at $t = 0.6667$ s. In the first simulation in Fig. 10(a) for conventional SHCM-PWM technique, during the transient, when the active and reactive powers are changed, more than two fundamental cycles are required to reach the steady state. The dc offset of the current $i_{\rm in}$ lasts for more than two cycles. The maximum dc offset shown in Table III is 43%−78%. This dc offset can lead to instability. The waveforms in Fig. 10(b) are with the proposed hybrid technique. During the transient, the active power and reactive power are changed separately within one cycle with the conditions defined in (18). As shown in the figure, $i_{\rm in}$ reaches the steady state within less than one cycle. The maximum 1.75%–8.5% dc offset is negligible as shown in Table III. The carrier frequency of PSPWM technique under dynamic condition is 240 Hz as derived in (21). The harmonic spectrum of $i_{\rm in}$ with the proposed technique, when the active and reactive power is 1000 W − 830 VAR, is shown in Fig. 10(c). The modulation index of $v_{\rm ac\text{-}CHB}$ is 2.399, which is within the modulation index range of conventional technique in Fig. 4. The harmonic spectrum of $i_{\rm in}$ with the proposed technique, when the active and reactive power is 520 W + 275 VAR, is shown in Fig. 10(d). The modulation index is 1.647, which is inside the extended modulation index range in Fig. 4. As shown in Fig. 10(c) and (d), with the proposed technique, the harmonic spectra of $i_{\rm in}$ can meet the IEEE 519 current harmonic limits.

In the second comparative simulations, the active and reactive power flowing from power grid to the converter changed from −800 W + 870 VAR to −500 W − 520 VAR at $t = 0.6023$ s and then changed back to −800 W + 870 VAR at $t = 0.6667$ s. In Fig. 11(a), for conventional SHCM-PWM technique, during the transient, when the active and reactive powers are changed, more than two fundamental cycles are required to reach steady state. A huge, 92%–94% dc offset shown in Table III is observed in the current $i_{\rm in}$ and it lasts for more than two cycles. This dc offset can lead to instability on the controller. The waveforms in Fig. 11(b) are with the proposed hybrid technique. During the transient, the active power and the reactive power are changed separately within one cycle with the conditions defined in (18). As shown in the figure, $i_{\rm in}$ reaches the steady state within less than one cycle. The maximum 1.4%–3.8% dc offset is negligible, as shown in Table III. The carrier frequency of PSPWM technique under dynamic condition is 240 Hz as derived in (21). The harmonic spectrum of $i_{\rm in}$ at −800 W + 870 VAR with a 1.52 modulation index, which is inside the extended modulation index range in Fig. 4, is shown in Fig. 11(c). The harmonic spectrum of $i_{\rm in}$ at −500 W − 520 VAR is shown in Fig. 11(d). The modulation index is 2.274, which is inside the conventional modulation index range in Fig. 4. It is obvious that the harmonics of $i_{\rm in}$ for both conditions meet the current harmonic limits of IEEE 519.

From Figs. 10(b) and 11(b), after one fundamental period, both the voltage and the current reach the steady state for these two transients, when the grid voltage is 110 V and $\Delta v_{\rm ac\text{-}Grid} = 0$.

The efficiencies of SHCM-PWM technique and PSPWM technique are compared when both of them meet the IEEE-519 current harmonic limits with the minimum number of switching transitions (frequencies). The minimum frequency for SHCM-PWM is 540 Hz. The minimum frequency for PSPWM is 4110 Hz, which can be calculated based on IEEE-519, (19),

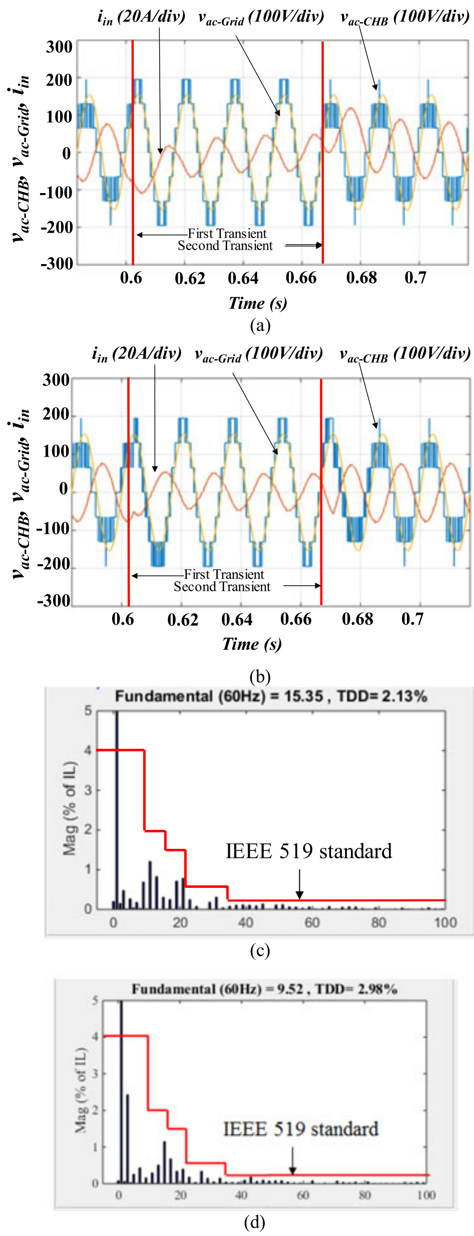

Fig. 11. Simulation results of the four-quadrant converter, when active and reactive power changes from −800 W + 870 VAR to − 500 W − 520 VAR and then back to −800 W + 870 VAR: (a) $V_{\text{ac-CHB}}$, $V_{\text{ac-Grid}}$, I_{in} with conventional technique, (b) $V_{\text{ac-CHB}}$, $V_{\text{ac-Grid}}$, I_{in} with the proposed hybrid SHCM-PWM and PSPWM technique, (c) the harmonic spectrum at −800 W + 870 VAR with the proposed hybrid technique, and (d) the harmonic spectrum at −500 W − 520 VAR with the proposed hybrid technique.

and the circuit parameters in Table II. The switching power loss P_{SW} of power devices is proportional to switching frequency f_s [18]

$$P_{\text{SW}} \propto f_s. \tag{22}$$

Because of this, the SHCM-PWM can significantly reduce the switching power loss. A comparison of the simulated switching power losses with SHCM-PWM and PSPWM techniques is shown In Table IV. The SHCM-PWM technique has lower

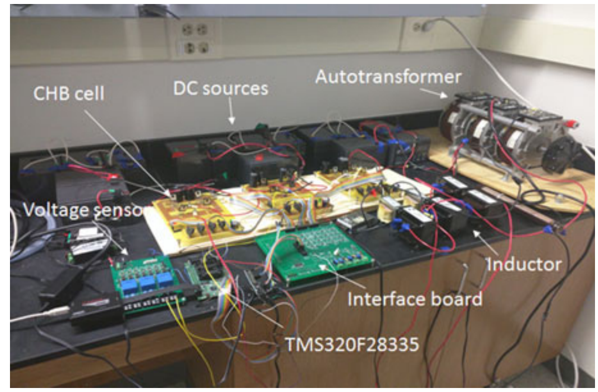

Fig. 12. Hardware prototype of the four-quadrant CHB used in the experiments.

switching power losses than PSPWM technique because it needs a lower switching frequency than PSPWM to meet IEEE-519.

V. Experimental Results

The proposed technique is further validated in experiments. A seven-level four-quadrant CHB converter, which has the same parameters as in simulations, with the proposed hybrid technique is developed in Fig. 12. The TMS320F28335 DSP is used in the prototype. Similar to Fig. 10, in the first comparative experiments, the active and reactive power flowing from power grid to the converter changed from 1000 W − 830 VAR to 520 W + 275 VAR and then changed back to 1000 W − 830 VAR. The transient periods are between two red lines. In Fig. 13(a), the conventional technique with SHCM-PWM took at least two fundamental cycles to reach the steady state. A 35%–65% dc offset is observed in i_{in} in Table V during the transient. This huge dc offset can lead to instability of controller and reduce the reliability of the semiconductor switches. In Fig. 13(b), for the proposed hybrid technique, which complies with the condition derived in (18), the d and q components each changed once in one cycle. It took less than one cycle to reach the steady state. The 2.5%–12% dc offset is much smaller than conventional technique, as shown in Table V. The switching frequency of PSPWM technique is 240 Hz as derived in (21). The current harmonic spectra of i_{in} in steady state at both 1000 W − 830 VAR and 520 W + 275 VAR are shown in Fig. 13(c) and (d), respectively. Both harmonic spectra can meet the IEEE 519 current harmonic limits. The modulation indices for both conditions are the same as the simulation results. This confirms the extended modulation index range in Fig. 4.

In the second comparative experiments in Fig. 14, the active and reactive power flowing from power grid to the converter changed from −800 W + 870 VAR to −500 W − 520 VAR and then changed back to −800 W + 870 VAR. As shown in Fig. 14(a), the conventional technique took at least two fundamental cycles to achieve the steady state. A 37%–60% dc offset is observed during the transient in Table V. In Fig. 14(b), the proposed hybrid technique took less than one cycle to reach steady state with only a 5%–5.8% dc offset during the transient. Fig. 14(c) and (d) shows the current harmonic spectra of i_{in} meet the IEEE 519 current harmonic limits under both conditions.

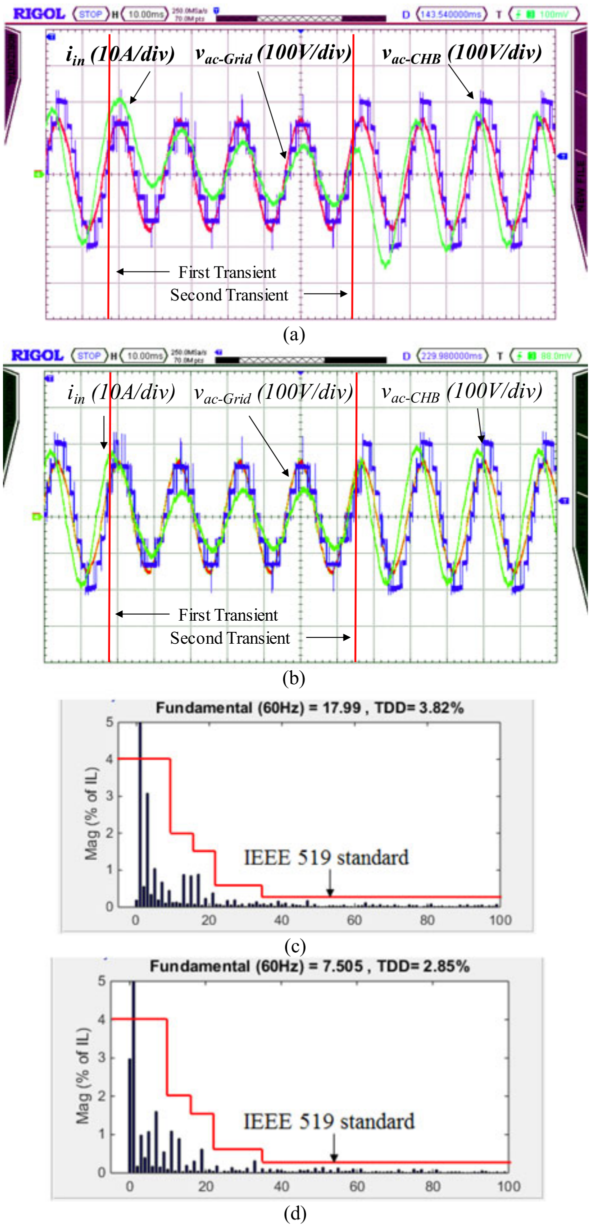

Fig. 13. Experimental results of the four-quadrant converter when active and reactive power changes from 1000 W − 830 VAR to 520 W + 275 VAR and then changes back to 1000 W − 830 VAR: (a) $V_{\text{ac-CHB}}$, $V_{\text{ac-Grid}}$, I_{in} with conventional technique, (b) $V_{\text{ac-CHB}}$, $V_{\text{ac-Grid}}$, I_{in} with proposed hybrid SHCM-PWM and PSPWM technique, (c) the harmonic spectrum at 1000 W − 830 VAR, and (d) the harmonic spectrum at 520 W + 275 VAR.

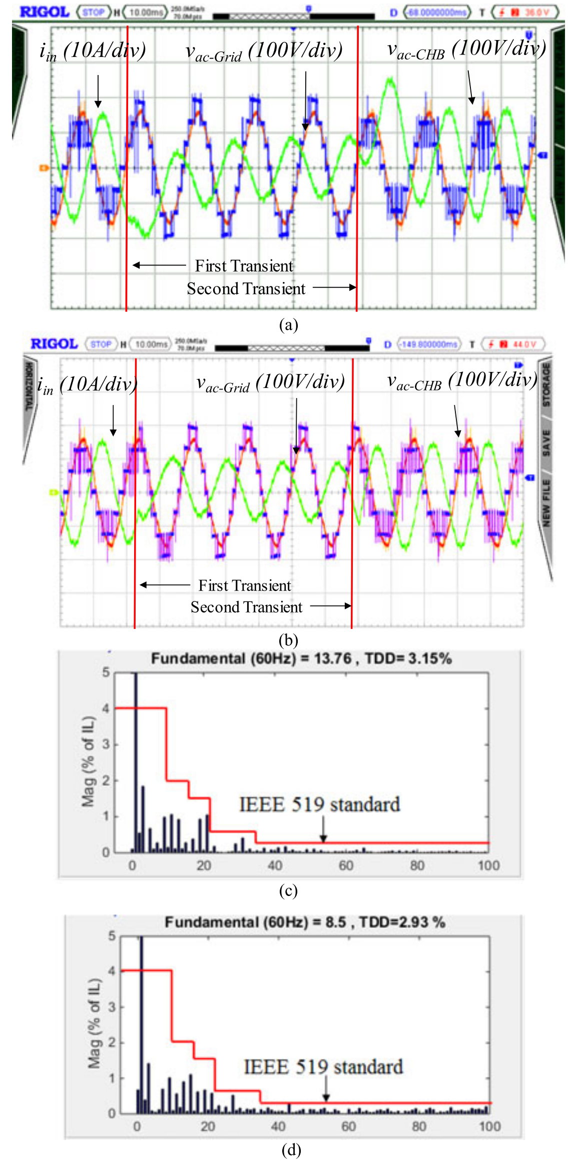

Fig. 14. Experimental results of the four-quadrant converter when active and reactive powers changes from −800W + 870 VAR to −500 W – 520 VAR and then changes back to −800 W + 870 VAR: (a) $V_{\text{ac-CHB}}$, $V_{\text{ac-Grid}}$, I_{in} with conventional technique, (b) $V_{\text{ac-CHB}}$, $V_{\text{ac-Grid}}$, I_{in} with the proposed hybrid SHCM-PWM and PSPWM technique, (c) the harmonic spectrum at −800 W + 870 VAR, and (d) the harmonic spectrum at −500 W – 520 VAR.

TABLE V
MAXIMUM DC OFFSET OF I_{IN} IN EXPERIMENTS WITH CONVENTIONAL AND THE PROPOSED TECHNIQUES

Experiment Number	First Transient (Conventional)	First Transient (Proposed)	Second Transient (Conventional)	Second Transient (Proposed)
First	65%	12%	35%	2.5%
Second	60%	5%	37%	5.8%

As proven by both experiment and simulation results, with the developed hybrid technique, the CHB rectifier can process four-quadrant active and reactive power with the extended modulation index, achieve fast dynamic response and meet IEEE-519 current harmonic limits.

It should be pointed out that, ideally, the proposed hybrid technique can achieve a transient free dynamic response; however, because of the nonideal component parameters, such as the variations of the dc-link voltages, the resistance of the inductor, the impedance of power grid, etc., there is still a small dc offset during the transient. However, compared with the conventional technique, the proposed hybrid technique significantly improves the dynamic response.

VI. Conclusions

In this paper, a hybrid modulation technique, which employs selective harmonic current mitigation PWM at the steady state and phase-shift PWM in transient, was proposed to process four-quadrant power, to achieve fast transient response, to increase the efficiency of the converter, to extend modulation index range, and to meet the IEEE-519 current harmonic limits. Both simulation and experimental results validate the proposed technique. It was shown that the proposed technique greatly reduces the dc offset and reduces transient response time of the injected currents. Moreover, the harmonic spectra of the injected current can meet IEEE 519 current limits at both steady and transient conditions. The modulation index range has been greatly extended with the proposed four-quadrant switching angel control technique for SHCM-PWM, so the SHCM-PWM can process a wide range of active and reactive power.

References

[1] S. Khomfoi and L. M. Tolbert, "Multilevel power rectifiers," in *Power Electronics Handbook*. Knoxville, TN, USA: Dept. Elect. Comput. Eng., Univ. Tennessee, 2007.

[2] M. S. A. Dahidah, G. Konstantinou, and V. G. Agelidis, "A review of multilevel selective harmonic elimination PWM: Formulations, solving algorithms, implementation and applications," *IEEE Trans. Power Electron.*, vol. 30, no. 8, pp. 4091–4106, Aug. 2015.

[3] L. He, J. Xiong, H. Ouyang, P. Zhang, and K. Zhang, "High-performance indirect current control scheme for railway traction four-quadrant converters," *IEEE Trans. Ind. Electron.*, vol. 61, no. 12, pp. 6645–6654, Dec. 2014.

[4] A. J. Watson, P. W. Wheeler, and J. C. Clare, "A complete harmonic elimination approach to DC link voltage balancing for a cascaded multilevel rectifier," in *IEEE Trans. Ind. Electron.*, vol. 54, no. 6, pp. 2946–2953, Dec. 2007.

[5] L. G. Franquelo, J. Napoles, R. C. P. Guisado, J. I. Leon, and M. A. Aguirre, "A flexible selective harmonic mitigation technique to meet grid codes in three-level PWM rectifiers," *IEEE Trans. Ind. Electron.*, vol. 54, no. 6, pp. 3022–3029, Dec. 2007.

[6] A. Moeini, H. Zhao, and S. Wang, "A current reference based selective harmonic current mitigation PWM technique to improve the performance of cascaded H-bridge multilevel active rectifiers," in *IEEE Trans. Ind. Electron.*, to be published.

[7] *IEEE Recommended Practices and Requirements for Harmonic Control in Electrical Power Systems*, New York, IEEE Std 519, 1992.

[8] A. Moeini, Z. Hui, and S. Wang, "High efficiency, hybrid selective harmonic elimination phase-shift PWM technique for cascaded H-bridge inverters to improve dynamic response and operate in complete normal modulation indices," in *Proc. IEEE Appl. Power Electron. Conf. Exp.*, Long Beach, CA, USA, 2016, pp. 2019–2026.

[9] M. Dabbaghjamanesh, A. Moeini, M. Ashkaboosi, P. Khazaei, and K. Mirzapalangi, "High performance control of grid connected cascaded H-bridge active rectifier based on type II-fuzzy logic controller with low frequency modulation technique," *Int. J. Elect. Comput. Eng.*, vol. 6, no. 2, pp. 484–494, 2016.

[10] H. Zhao and S. Wang, "A four-quadrant modulation technique to extend modulation index range for multilevel selective harmonic elimination/compensation using staircase waveforms," *IEEE J. Emerg. Sel. Topics Power Electron.*, vol. 5, no. 1, pp. 233–243, Mar. 2017.

[11] A. Moeini, H. Iman-Eini, and M. Bakhshizadeh, "Selective harmonic mitigation-pulse-width modulation technique with variable DC-link voltages in single and three-phase cascaded H-bridge inverters," *IET Power Electron*., vol. 7, no. 4, pp. 924–932, Apr. 2014.

[12] S. Wang, R. Crosier, and Y. Chu, "Investigating the power architectures and circuit topologies for megawatt superfast electric vehicle charging stations with enhanced grid support functionality," in *Proc. IEEE Int. Elect. Veh. Conf.*, Greenville, SC, USA, 2012, pp. 1–8.

[13] B. Alamri, A. Sallama, and M. Darwish, "Optimum SHE for cascaded H-bridge multilevel inverters using: NR-GA-PSO, comparative study," in *Proc. 11th IET Int. Conf. AC DC Power Transmission*, Birmingham, U.K., 2015, pp. 1–10.

[14] H. Taghizadeh and M. Tarafdar Hagh, "Harmonic elimination of cascade multilevel inverters with nonequal DC sources using particle swarm optimization," *IEEE Trans. Ind. Electron.*, vol. 57, no. 11, pp. 3678–3684, Nov. 2010.

[15] S. Beheshtaein, "Multi-objective selective harmonic mitigation for cascaded H-bridge multilevel inverters connected to photovoltaic systems using hierarchical multi-output support vector regression," in *Proc. 39th Annu. Conf. IEEE Ind. Electron. Soc.*, Vienna, 2013, pp. 72–79.

[16] V. G. Agelidis, A. I. Balouktsis, and M. S. A. Dahidah, "A five-level symmetrically defined selective harmonic elimination PWM strategy: Analysis and experimental validation," *IEEE Trans. Power Electron.*, vol. 23, no. 1, pp. 19–26, Jan. 2008.

[17] D. G. Holmes and T. A. Lipo, *Pulse Width Modulation for Power Converters: Principles and Practice*. New York, NY, USA: Wiley, 2003.

[18] Y. Xiong, S. Sun, H. Jia, P. Shea, and Z. John Shen, "New physical insights on power MOSFET switching losses," *IEEE Trans. Power Electron.*, vol. 24, no. 2, pp. 525–531, Feb. 2009.

Amirhossein Moeini (S'16) received the B.Sc. degree in electrical engineering from the University of Guilan, Rasht, Iran, in 2011, and the M.Sc. degree in power electronics and electrical machines from the University of Tehran, Tehran, Iran, in 2013. He is currently working toward the Ph.D. degree in the Power Electronics and Electrical Power Research Laboratory, University of Florida, Gainesville, FL, USA.

His current research interests include modeling and control of power electronic converters, FACTS devices, power quality, evolutionary optimization methods, and optimal modulation techniques.

Hui Zhao (S'14) received the bachelor's and master's degrees in electrical engineering from Huazhong University of Science and Technology, Wuhan, China, in 2010 and 2013, respectively. He is currently working toward the Ph.D. degree in the Electrical and Computer Engineering Department, University of Florida, Gainesville, FL, USA.

He served a summer internship at the General Electric (GE) Global Research Center Shanghai in 2013. He has authored or coauthored several IEEE conference and Transaction papers.

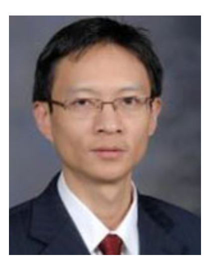

Shuo Wang (S'03–M'06–SM'07) received the Ph.D. degree from Virginia Polytechnic Institute and State University (Virginia Tech), Blacksburg, VA, USA, in 2005.

Since 2015, he has been an Associate Professor with the Department of Electrical and Computer Engineering, University of Florida, Gainesville, FL, USA. From 2010 to 2014, he was with The University of Texas at San Antonio, San Antonio, TX, USA, first as an Assistant Professor and later as an Associate Professor. From 2009 to 2010, he was a Senior Design Engineer with GE Aviation Systems, Vandalia, OH, USA. From 2005 to 2009, he was a Research Assistant Professor at Virginia Tech. He has authored or coauthored more than 140 IEEE journal and conference papers and holds 8 U.S. patents.

Dr. Wang received the Best Transactions Paper Award from the IEEE Power Electronics Society in 2006 and two William M. Portnoy Awards for papers published by the IEEE Industry Applications Society in 2004 and 2012. In 2012, he received the prestigious National Science Foundation CAREER Award. He is an Associate Editor for the IEEE Transactions on Industry Applications and was a Technical Program Co-Chair for the IEEE 2014 International Electric Vehicle Conference.